Fine-scale depth structure of pelagic communities throughout the global ocean based on acoustic sound scattering layers

Running page header: **Sound scattering layer depth structure**

Roland Proud[1*], Martin J. Cox[2], Camille Le Guen[1] & Andrew S. Brierley[1]

[1]Pelagic Ecology Research Group, Scottish Oceans Institute, Gatty Marine Laboratory, School of Biology, University of St Andrews, KY16 8LB, UK.

[2]Australian Antarctic Division, Kingston, Tasmania, 7050, Australia.

*rp43@st-andrews.ac.uk

Abstract

Most biomass in the mesopelagic zone (200 – 1000 m) comprises zooplankton and fish aggregated in layers known as sound scattering layers (SSLs; they scatter sound and are detectable using echosounders). Some of these animals migrate vertically to and from the near surface on a daily cycle (diel vertical migration; DVM), transporting carbon between the surface and the deep ocean (biological carbon pump; BCP). To gain insight to potential global variability in the contribution of SSLs to the BCP, and to pelagic ecology generally (SSLs are likely prey fields for numerous predators), we report here regional-scale (90000 km2) community depth structure based on the fine-scale (10s of m) vertical distribution of SSLs. We extracted SSLs from a near-global dataset of 38 kHz echosounder observations and constructed local (300 km by 300 km) SSL depth and echo intensity (a proxy for biomass) probability distributions. The probability distributions fell into six spatially coherent regional-scale SSL probability distributions (RSPDs). All but one RSPD exhibited clear DVM, and all RSPDs included stable night-time resident deep scattering layers (DSLs; SSLs deeper

than 200 m). Analysis of DSL number and stability (probability of observation at depth) revealed 2 distinct DSL types: 1.) Single-Shallow DSL (single DSL at c. 500 m), and 2.) Double-Deep DSL (two DSLs at c. 600 and 850 m). By including consideration of this fine-scale depth structure in biogeographic partitions and ecosystem models, we will better understand the role of mesopelagic communities in pelagic food-webs and consequences for them of climate change.

Keywords: Biogeography, DVM, Acoustics, Water column, DSL, Mesopelagic

Introduction

The biological carbon pump (BCP), mediated by the regular vertical migrations of mesopelagic organisms, transfers large quantities of carbon from the atmosphere in to the deep ocean (Anderson et al. 2018). It is estimated that the atmospheric concentration of carbon dioxide is presently about 200 ppm lower than it would otherwise be in the absence of the BCP (Parekh et al. 2006). The diel vertical migration (DVM) that is integral to the operation of the BCP can be detected, using scientific echosounders, as the upward and downward migrations at dusk and dawn of the open-ocean communities that comprise acoustic deep scattering layers (DSLs; sound scattering layers deeper than 200 m). The fine-scale (10s of m) depth structure of these communities will likely impact the efficiency of the BCP (see Klevjer et al. 2016) and the foraging behaviour of air-breathing deep-diving predators including *Mirounga* sp. (Northern and Southern Elephant Seals) and *Aptenodytes patagonicus* (King penguins) (Scheffer et al. 2010, Boersch-Supan et al. 2012). It is therefore

important to consider regional variability in open-ocean community depth structure in studies of open-ocean ecology and in the design of open-ocean ecosystem/biogeochemical models such as SEAPODYM, Atlantis and MIZER (Lehodey et al. 2008, Fulton et al. 2011, Trebilco et al. 2013, Scott et al. 2014), which are in turn important components of climate models (Giering et al. 2014). Variability in depth structure should also be considered when partitioning the ocean into ecological regions (Proud et al. 2017, Sutton et al. 2017).

Vertical structure of water-column communities

From the sea-surface to 1000 m deep, the pelagic zone (i.e. the water-column away from the seabed) can be divided into two zones, the epipelagic (0 to 200 m) and the mesopelagic (200 to 1000 m). The epipelagic contains an illuminated mixed-layer that is isothermal and usually bounded by a steep seasonal thermocline, which is variable in depth. The epipelagic is the site of oceanic primary production (PP), the magnitude of which is a function of light intensity, temperature and nutrient availability (via mixing). PP varies widely both geographically and over time (Boyce et al. 2010, 2012), and PP variability has been one prominent basis for partitioning the global ocean into ecological regions, such as the 'provinces' derived by Longhurst (Longhurst 2007). The mesopelagic is typically colder than the epipelagic, and seawater there is denser. Key inhabitants of the mesopelagic are the zooplankton, squid and small bony fish that aggregate in layers and which generally migrate daily (i.e. undertake DVM) upwards towards the surface at dusk to feed before returning to depth at dawn (Bianchi et al. 2013, Bianchi & Mislan 2016). However, not all organisms migrate daily, and 'resident' night-time mesopelagic communities have often been observed (Koslow et al. 1997, Flynn & Kloser 2012). Generally, the migrating community follows low-light intensity isolumes, such that they ascend to feed whilst minimising the risk of being

detected by visual predators (Hays, 2003). Daily movements and rest periods at depth facilitates transport of carbon, nutrients and energy (via respiration and excretion) from the surface to deep water (Schnetzer & Steinberg 2002). Seasonal community movements including overwintering at depth by copepods also contribute to nutrient and energy flux (Jónasdóttir et al. 2015).

Deep Scattering Layers

DSLs, which form in the mesopelagic zone, take their name from the fact that they scatter sound. A consequence of this is that they can be detected using active acoustic sampling (scientific echosounding). The depth at which DSLs are located varies geographically and seasonally (Anderson et al. 2005, Kloser et al. 2009, Irigoien et al. 2014, Knutsen et al. 2017, Proud et al. 2017). This variability is thought to be predictable, since observed depths of DSLs have been linked to environmental drivers such as seawater density (Godø et al. 2012), light intensity (Hays 2003, Aksnes et al. 2017, Proud et al. 2017), oxygen concentration (Bianchi et al. 2013; Klevjer et al. 2016) and wind-driven mixing (Proud et al. 2017). Furthermore, regional variability in the intensity of echoes from DSLs, a rough proxy for biomass, has been linked to PP in the waters above and to temperature (Irigoien et al. 2014, Fennell & Rose 2015, Proud et al. 2017). There is often more than one DSL in a given location (Andreeva et al. 2000), and DSLs at different depths likely comprise different communities (the stacked DSLs can be considered as rungs in Vinogradov's (1968) 'ladders of migration'). The vertical distributions of these multiple DSLs can shift at twilight, with some migrating in unison, some remaining stationary, some merging, and some splitting, such that there are distinct day and night patterns (e.g. Klevjer et al. 2012). These complex and variable depth structures vary globally and may well be intimately linked to

concomitant environmental variability. By characterising the form and variability of these depth structures, we inadvertently characterise complex and distinct environments, which may enable improved partitioning of the ocean into biogeographic regions.

Biogeography

Historically, biogeographic partitioning of the ocean was generally performed using just biological data (Brinton 1962, Alvarino 1965, Briggs 1974, Semina 1997), but more recent classifications have been able to capitalize on the availability of open-access data and to incorporate numerous data sources (including biological, chemical and physical) into their partitioning algorithms (Longhurst 2007, Proud et al. 2017, Sayre et al. 2017, Sutton et al. 2017). Distributions and abundances of species and 'environmental' parameters vary with depth, so it is not necessary to expect that the same spatial grid of classification at the surface, say, would pertain in the mesopelagic. Further, the number of separate classes, units, or provinces that can be identified/discriminated depends on many factors including chosen scale and number of variables considered. In most cases the number of separations can be considered to be an arbitrary, artificial construct, and is usually selected for a specific purpose e.g. management (e.g. Sayre et al. 2017) or research applications. Biogeographies vary by depth strata, from surface and epipelagic classification (Longhurst 2007, Oliver & Irwin 2008, Spalding et al. 2012), mesopelagic and water-column (Flynn & Marshall 2013, Proud et al. 2017, Sayre et al. 2017, Sutton et al. 2017) to seabed (UNESCO 2009, Watling et al. 2013). However, none have included detailed (10s of m) water-column community depth structure because data have not been readily available.

Hypothesis and objectives

The biophysical drivers of DSL depth and echo intensity (a proxy for biomass; Proud et al. 2018) have been used to demark global biogeographies (Proud et al. 2017). We therefore hypothesise that distinct communities, with distinct depth preferences, exist and that these preferences lead to spatially coherent vertical structuring at regional-scales. To test this hypothesis, our approach was as follows: 1.) extract sound scattering layer (SSL; non-depth-specific scattering layer) depth, thickness and echo intensity (between 0 to 1200 m) from globally collated 38 kHz echosounder data using the SSL extraction method (SSLEM, Proud et al. 2015); 2.) produce local (300 km by 300 km) SSL probability distributions (SPD), which provide, for a given area, the probability of observing an SSL at a specific depth and echo intensity value; 3.) cluster the SPDs by likeness and derive regional-scale SSL probability distributions (RSPDs), and 4.) categorize RSPDs by DSL depth structure and vertical stability, defined as the probability of DSL observation at its principal, or most common, depth (e.g. where a DSL is always observed at a certain depth for a specific RSPD, DSL vertical stability would equal 1).

Method

SSLs were extracted from an extensive acoustic dataset (3196 38 kHz echograms; equal to 380 days of observations), spatially binned into 300 km by 300 km cells (90000 km^2), grouped by day and night, and summarised by depth and mean volume backscattering strength (MVBS, dB re $1m^{-1}$, Maclennan et al. 2002) SSL probability distributions (SPDs). SSLs that had a mean depth > 200 m were defined as deep scattering layers (DSLs). Cluster

136 analysis was used to group similar SPDs in space, and regional-scale SPDs were defined,
137 enabling inferences on the underlying biological communities to be made.

138

139 *Acoustic data*

140 38 kHz echosounder observations, recorded between 2006 and 2015, were collated from
141 the British Oceanographic Data Centre (BODC, www.bodc.ac.uk, 2014), the British Antarctic
142 Survey (BAS 2015, www.bas.ac.uk), the Pelagic Ecology Research Group (PERG), the
143 Integrated Marine Observing System (IMOS 2013, www.imos.org.au) and the Surface Mixed
144 Layer Evolution at Sub-mesoscales Cruise (SMILES 2015). Seasonal coverage was variable,
145 ranging from near uniform sampling with full seasonal coverage in the South Indian Ocean,
146 to regions with lower sample coverage (1-2 seasons) in the polar and North Pacific regions
147 (polar regions are not typically sampled during winter due to sea ice cover).

148 Data were calibrated and noise was removed (see Proud et al. 2017 supplemental
149 information for details of data processing). SSLs persisting for longer than 30 minutes were
150 extracted and characterised using the SSL extraction method (SSLEM, Proud et al. 2015).
151 Individual SSLs were described by their mean depth, thickness and MVBS, and binned by
152 geographic location onto a uniform global 300 km by 300 km grid (where seabed depth >
153 1000 m) as per the spatial scale applied by Proud et al. (2017). Gridded SSLs were grouped
154 by day and night periods (demarked using local sunrise and sunset times) and summarised
155 by depth and MVBS SSL probability distributions (SPDs).

156

157

158 *Sound scattering layer probability distributions*

159 Following Proud et al. (2017), we define the probability (P) of observing an SSL at a specific
160 depth (z) and MVBS value as

161 $$\mathrm{P_{z,MVBS}} = \frac{\mathrm{obs_{z,MVBS}}}{\mathrm{se_z}}, \quad (1)$$

162 where $\mathrm{obs_{z,MVBS}}$ is the total time of SSL observation (s) by depth (0 to 1200 m by 5 m
163 intervals) and MVBS level (-50 dB re $1\mathrm{m}^{-1}$ to -100 dB re $1\mathrm{m}^{-1}$ by 2 dB re $1\mathrm{m}^{-1}$ intervals) and
164 $\mathrm{se_z}$ is the sampling effort (s) by depth i.e. for each depth interval the probability of SSL
165 observation (including the probability of no observation) sums to one. Calculating P over the
166 entire depth and MVBS range yielded an SSL probability distribution (SPD) for each
167 geographic cell for both day and night.

168 *Seasonal coverage index (SCI)*

169 To quantify the temporal distribution of echosounder observations for each SPD, a seasonal
170 coverage index (SCI), given by,

171 $$\mathrm{SCI} = \sum_{\mathrm{i}=1}^{4} \mathrm{se_i} \Big/ max([\mathrm{se_1}, \mathrm{se_2}, \mathrm{se_3}, \mathrm{se_4}]) \quad (2)$$

172 was calculated, where $\mathrm{se_i}$ is the sampling effort (s) for each season, represented by the
173 integer i, ranging from 1 (spring) to 4 (winter) and *max* is a function that returns the
174 maximum value of a given vector. For an SPD where all observations were made in a single
175 season, SCI would equal 1, whereas for an SPD where the sampling effort for all four
176 seasons was the same (uniform distribution), SCI would equal 4.

177

178 *Epipelagic and mesopelagic nautical area scattering coefficient*

179 The total amount of scattered energy produced per square nautical mile over a depth range
180 is known as the nautical area scattering coefficient (NASC, s_A, m^2 nmi^{-2}, Maclennan et al.,
181 2002). The NASC values over the epipelagic (s_{epi}, 0 – 200 m, m^2 nmi^{-2}) and mesopelagic
182 (s_{meso}, 200 – 1000 m, m^2 nmi^{-2}) zones (in 5 m depth bins in both) are given by

183 $$s_{epi} = \sum_{j=0}^{40} \left(\sum_{i=0}^{25} \left(P_{\mathbf{Z}[j],\mathbf{M}[i]} \times 10^{(\mathbf{M}[i]/10)} \right) \right) \times 4\pi \times 1852^2 \quad (3)$$

184 and

185 $$s_{meso} = \sum_{j=40}^{200} \left(\sum_{i=0}^{25} \left(P_{\mathbf{Z}[j],\mathbf{M}[i]} \times 10^{(\mathbf{M}[i]/10)} \right) \right) \times 4\pi \times 1852^2 \quad (4)$$

186 respectively, where j is an index for the vector **Z**, which is consistent of 200 equally spaced
187 SSL depth bins (0 – 1000 m by 5 m) and i, is an index for the vector **M**, which comprises 25
188 equally spaced SSL MVBS bins (-50 dB re $1m^{-1}$ to -100 dB re $1m^{-1}$ by 2 dB re $1m^{-1}$).

189

190 *Principal deep scattering layer depth, MVBS and stability*

191 The probability of observing an SSL at a specific depth, $P_{\mathbf{Z}[j]}$, defined as the vertical stability
192 of an SSL, is given by

193 $$P_{\mathbf{Z}[j]} = \sum_{i=0}^{25} P_{\mathbf{Z}[j],\mathbf{M}[i]}. \quad (5)$$

194 The principal or most common DSL depth, Z_{PDSL} (see Proud et al. 2017), was determined by
195 finding the maximum value of $P_{\mathbf{Z}[j]}$ between 200 and 1000 m (**Z**[40] to **Z**[200]):

196 $$\mathrm{P}_{\mathbf{Z}[40:200]} = \left\{\mathrm{P}_{\mathbf{Z}[40]}, \mathrm{P}_{\mathbf{Z}[41]}, \mathrm{P}_{\mathbf{Z}[42]} \ldots, \mathrm{P}_{\mathbf{Z}[199]}\right\}, \quad (6)$$

197 $$\mathrm{P}_{\mathrm{PDSL}} = max\left(\mathrm{P}_{\mathbf{Z}[40:200]}\right), \quad (7)$$

198 $$\mathrm{Z}_{\mathrm{PDSL}} = \mathbf{Z}\left[argmax\left(\mathrm{P}_{\mathbf{Z}[40:200]}\right)\right], \quad (8)$$

199 where P_{PDSL} is the probability of observing the principal DSL defined here as DSL vertical
200 stability and *argmax* is a function that returns the index of the maximum value. For
201 example, in the case where a DSL was always observed at a specific depth, P_{PDSL} would equal
202 1, i.e. the DSL was always observed at Z_{PDSL} and therefore had a high vertical stability.
203 Similarly, given that a DSL has been observed, the most likely MVBS value of the principal
204 DSL, $MVBS_{PDSL}$, is given by

205 $$\mathrm{P}_{\mathbf{M}[\mathrm{i}]} = \sum_{\mathrm{j}\,=\,40}^{200} \mathrm{P}_{\mathbf{Z}[\mathrm{j}],\mathbf{M}[\mathrm{i}]} \Bigg/ \sum_{\mathrm{j}=40}^{200} \left(\sum_{\mathrm{i}=0}^{25} \left(\mathrm{P}_{\mathbf{Z}[\mathrm{j}],\mathbf{M}[\mathrm{i}]}\right) \right), \quad (9)$$

206 $$\mathrm{P}_{\mathbf{M}[0:25]} = \left\{\mathrm{P}_{\mathbf{M}[0]}, \mathrm{P}_{\mathbf{M}[1]}, \mathrm{P}_{\mathbf{M}[2]} \ldots, \mathrm{P}_{\mathbf{M}[24]}\right\}, \quad (10)$$

207 $$\mathrm{P}_{\mathrm{PMVBS}} = max\left(\mathrm{P}_{\mathbf{M}[0:25]}\right), \quad (11)$$

208 $$\mathrm{MVBS}_{\mathrm{PDSL}} = \mathbf{M}\left[argmax\left(\mathrm{P}_{\mathbf{M}[0:25]}\right)\right], \quad (12)$$

209 where P_{MVBS} is the probability of the principal DSL having a MVBS value of $MVBS_{PDSL}$.

210 *Clustering sound scattering layer probability distributions (SPDs)*

211 A distance measure was derived to determine the similarity between each SPD. Since the
212 SPDs were all constructed from a set of discrete probabilities, with values between 0 and 1
213 and with just one value per depth/MVBS bin, a simple matrix subtraction was used to
214 calculate a relative distance measure,

$$\mathrm{dist}_{AB} = \sum \mathrm{abs}(\mathbf{A} - \mathbf{B}), \quad (13)$$

where **A** and **B** are 2-dimensional arrays (SPDs) and $\mathrm{dist}_{\mathbf{AB}}$ is a relative distance measure between **A** and **B**. The maximum value of dist_{AB} is equal to the size of the SPD arrays (240 depth bins × 25 MVBS bins = 6000 cells) i.e. where the probability of SSL observation at a specific depth and MVBS combination in **A** = 0, the probability for the same depth and MVBS values in **B** would equal 1. By the same logic, where two SPDs are identical (i.e. where the probability of observing SSLs across all depth and MVBS combinations is the same) dist_{AB} = 0.

Using Eq. 13, a dissimilarity matrix **D** that contained the pairwise distances between all daytime SPDs (total number of SPDs = X) was constructed. Classical multi-dimensional scaling (MDS, Hout et al. 2013) was applied to reduce the data to a smaller number of dimensions, improving computational efficiency. From the resulting configuration matrix, an appropriate number of dimensions, D, was assigned by evaluating values of stress (the degree of correspondence between the distances of the original data and MDS map, where a value of 0 is perfect correspondence). A k-means clustering algorithm (Hartigan & Wong 1979) was applied to the resultant reduced dataset (size = X by D) to determine the natural number of groupings or clusters that were evident within the data. The optimum number of clusters was selected by identifying interruptions, or elbow-like features, in the Log-Likelihood (LL) trend (e.g. Sugar 1998). The algorithm was run for a range of k clusters (2 – 20), where at each step the LL value was determined (Eq. 14 and 15) to enable model assessment:

$$P(x|u) = \frac{e^{-\sum_{d \in D}(u_d - x_d)^2}}{\sum_u e^{-\sum_{d \in D}(u_d - x_d)^2}}, \quad (14)$$

$$\mathrm{LL} = \sum_{\mathrm{x} \in \mathrm{X}} \log max\,(\mathrm{P}(\mathrm{x}|\mathrm{u})), \quad (15)$$

where $\mathrm{P}(\mathrm{x}|\mathrm{u})$ is the probability of sample x (i.e. a single SPD) belonging to model u (k-means model).

Regional-scale sound scattering layer probability distributions (RSPDs)

The resultant k-clusters, consisting of n cluster members (SPDs formed from observations made within a single 300 km by 300 km cell) were merged to form new 'regional-scale' SPDs with larger spatial coverage (equal to n × 90000 km^2) by matrix addition. This operation was carried out by adding the underlying data ($obs_{z,MVBS}$, see Eq. 1) for all the SPDs in each cluster together, and then determining a new set of probabilities by applying new values of se_z to Eq. 1; this accounted for differences in sampling effort between cluster members. The merged clusters of SPDs were termed 'regional-scale SSL probability distributions' (RSPDs) and are associated spatially with individual cluster members. Finally, a local neighbourhood dilation filter (3 x 3 cells) was passed over the spatial grid of cells labelled by cluster number (k), and the centre value of the filter (either a cluster number or an unlabelled cell) was replaced with the maximum value calculated over the local neighbourhood. This filtering process removed anomalies and smoothed spatial transitions between RSPDs.

Results

In total, 39455 SSLs were extracted from the acoustic survey data via the SSLEM (Proud et al. 2015), including 26474 DSLs, and summarised by a set of metrics (depth, thickness and

MVBS). The SSL metrics were split by day and night and assigned to 297 unique 300 km by 300 km cells (these equate to c. 9% of the surface of the global open-ocean where seabed depth > 1000 m). SSL probability distributions (SPDs) were determined for each cell, and a distance measure was computed resulting in a dissimilarity matrix, **D**, with 297 rows and columns. The MDS analysis of **D** indicated that for a stress value of 0.1 (Kruskal 1964), **D** could be reduced from 297 dimensions to 37. The lower dimensional representation of the data, **D'**, accounted for 72% of the variance.

K-means clustering was applied to **D'** and using calculated values of the Log-Likelihood (Eq. 15), a six-cluster model was selected. An elbow-like feature was apparent when fitting six clusters (Fig. 1), increasing the value of the Log-Likelihood away from the decreasing trend; this feature indicated that there was a better than expected fit at this scale. As the number of clusters increased, particularly towards 15, more of these features appeared. Since in this study we were interested in regional-scale trends, taking the first natural grouping was appropriate. For the six-cluster model, 89% of the SPDs were assigned to a cluster with a probability (Eq. 14) that was at least twice the value of the next best selection, indicating a good fit.

[Figure1]

DSL vertical stability and sampling effort of SPD cluster members

Sampling effort per SPD ranged between c. 1 hour and 175 hours, and DSL vertical stability (P_{PDSL}) ranged between c. 0.32 and 1 (Fig. 2). DSLs were typically less stable during the night-time than the day and the lowest values of DSL vertical stability occurred in summer (Fig. 2). DSLs in clusters 1, 2, 4 and 5 were the most vertically stable, whereas in cluster 6 DSLs were highly unstable across the full range of sampling effort values.

[Figure 2]

Geographical distribution of SPD clusters

The SPD cluster members were plotted in space, revealing the underlying spatial affiliation of the echosounder observations (Fig. 3). The clusters formed large-scale spatially aggregated regions (Fig. 3). Cluster 6 was located mostly at higher latitudes, typically lying poleward of 40° latitude in both hemispheres. Cluster 3 formed a single region within the south Indian Ocean. The other clusters occurred at mid to low latitudes forming sub-regions both north and south of the equator (Fig. 3).

[Figure 3]

Regional-scale SSL probability distributions

SPDs were merged by cluster to form six distinct RSPDs (Fig. 4). RSPDs 1 to 5 exhibited strong compact trunk-like features in depth-MVBS space (Fig. 4). MVBS values of these RSPDs varied by a factor of 10 from RSPD1 ($MVBS_{PDSL}$ = -67 dB re $1m^{-1}$) to RSPD5 ($MVBS_{PDSL}$ = -77 dB re $1m^{-1}$). There was also an increase in backscattering intensity from day to night at the surface and a decrease in the mesopelagic depth zone, indicating DVM (Table 1).

[Figure 4]

All RSPDs had relatively stable depth structures during both day and night (Fig. 4) i.e. in all regions there was a component of the DSL assemblage that did not migrate, suggesting that 'resident' night-time DSLs are a ubiquitous feature of open-ocean pelagic ecosystems. This phenomenon could be explained by a component of the DSL consisting of either a temporary (e.g. through ontogenetic migration) or permanent (e.g. non-migrating fish species) resident mesopelagic community, or by asynchronous vertical migration (e.g. Dupont et al. 2009) where individuals of a given species behave as individuals, each selectively undertaking migration (intermittently or opportunistically) at a time cued by some individual trigger (e.g. predation pressure/food availability).

RSPD6, by contrast, was characterised by a broad, shallow probability distribution (Fig. 4), i.e. SSLs varied substantially in both depth and MVBS and there was no common structure. This RSPD arises from seasonally-limited sampling, so is not an artefact caused by blurring of temporal variability (Table 1, SCI = 1.8). It is formed from cells with low DSL vertical stability

(Fig. 2) and cells that contain relatively low MVBS SSLs (< -85 dB re $1m^{-1}$, see Fig. 4). RSPD6 MVBS increased from day to night in the mesopelagic (Table 1).

[Table 1]

Depth structure and DSL stability of RSPDs

RSPDs were ranked by s_{meso}, which is reflected by the decreasing value of $MVBS_{PDSL}$ (Table 1 and Fig. 5) from RSPD1 to 6. Analysis of the mesopelagic depth structure (number and depth of DSLs) and DSL vertical stability ($P_{z[40-200]}$, see Eq. 5), enabled categorisation of the RSPDs into 3 DSL types: 1.) Single-Shallow DSL (SS-DSL: RSPD1, 3 and 5), a single DSL at c. 500 m, 2.) Double-Deep DSL (DD-DSL: RSPD2 and 4), two DSLs at c. 600 m and 850 m and 3.) Unclassified DSL (U-DSL: RSPD6), highly variable depth structure and/or low (< -85 dB re $1m^{-1}$) MVBS values (Table 1, Fig. 2, 4 and 5).

[Figure 5]

Discussion

The RSPDs defined here give new insight to fine-scale (10s of m) depth structure of open-ocean communities and their day-to-night vertical stability (i.e. probability of observation at depth) and MVBS variability. They provide evidence that regional-scale spatially coherent community depth structures exist between 0 and 1200 m (Fig. 3 and 4). Since DSL metrics (e.g. Z_{PDSL} and $MVBS_{PDSL}$, see Table 1) are characteristics of the underlying mesopelagic

biological communities and that similar partitions arise from environmentally-based regionalisations (e.g. Longhurst provinces), then the observed cohesion here is likely to be due to environmental control. The between-region differences in DSL vertical stability and MVBS variability (Fig. 2, 4 and 5) are not artefacts of uneven sampling effort (see SCI in Table 1 and Fig. 2). The most vertically stable region was RSPD4 (defined by highest P_{PDSL} values, see Table 1) which occurred in the Southern Indian Ocean (Fig. 3), the area for which we have full seasonal sampling coverage (Table 1, SCI = 3.1). Conversely, the high vertical instability in the polar regions was evident in our seasonally-restricted data (we do not have data for the logistically-challenging winter period, see Table 1, RSPD6, SCI = 1.8). All RSPDs include resident night time DSLs which adhere to their daytime depth (Fig. 4). Spatial variability in DSL number and fine-scale depth structure will impact predator-prey interactions in pelagic food-webs and carbon transfer in the water-column via the biological carbon pump (Klevjer et al. 2016). Such variability should be considered in ocean partitioning schemes and in the design of mesopelagic components of ecosystem and biogeochemical models.

Implications for predator-prey interactions

DSL inhabitants (e.g. micronektonic organisms such as mesopelagic fish) represent a potentially rich food resource for both epipelagic predators (e.g. southern bluefin tuna (*Thunnus maccoyii*) and Pacific bluefin tuna (*Thunnus orientalis*); Bestley et al. 2008) at night and deep-sea consumers during the day (Hazen & Johnston 2010). Variability in daytime and night-time depth of DSLs, spatially characterised by RSPDs (Fig. 4), will likely impact the energy budgets of their inhabitants and deep-diving air-breathing predators (e.g. Southern

Elephant seals *Mirounga leonin*) for which DSLs constitute a dynamic prey-landscape (Boersch-Supan et al. 2012). For active vertical migrators, the opportunity to feed (and digest) in shallow, warm and productive waters may bring metabolic advantages that outweigh the cost of migration. For predators, however, the fact that potential prey biomass is deep during the day may effectively take it out of their reach: prey may exist but be inaccessible.

Predators adjust the time allocated to foraging according to the prey patch quality (Schoener 1979, Mori & Boyd 2004). Deep-diving air-breathing predators that are constrained by their oxygen requirements have been observed to rely on spatially predictable foraging grounds (Brown 1980, Charrassin & Bost 2001). Variation in prey availability leads predators to adjust their foraging behaviour and/or location, affecting their foraging success, which in turn has an impact on survival, breeding success, and eventually population abundance (New et al. 2014). Mesopelagic fish are a key component of the DSL as well as an important prey item for King penguins and Southern Elephant seals (Olsson & North 1997, Vacquié-Garcia et al. 2015). Both Southern Elephant seals and King penguins routinely dive to depths coincident with the DSL although direct evidence for foraging on DSLs by these species remains lacking. King penguins can dive down to depths of c. 400 m (Charrassin et al. 2002) and Southern Elephant seals have dive ranges beyond the mesopelagic zone (down to 2000 m; McIntyre et al. 2010). If they do feed upon DSLs, variation in DSL depth will impact the energy expenditure of their dives.

The daytime vertical range of DSLs in RSPD1, 3 and 5 extends to c. 400 m at their shallowest extent, whereas in RSPD2 and 4, DSLs reside slightly deeper at their shallowest extent (c. 500 m, see Fig. 4). Geographically, the only RSPDs within the latitudinal feeding range of

King penguins (i.e. south of the polar front) are the shallower DSLs (e.g. RSPD5 see Fig. 3). It is perhaps no coincidence that at the far extent of the King penguin's diving range, prey biomass starts to increase because predation pressure upon DSL occupants is reduced. Vertical zonation is a common phenomenon in the marine realm. The most readily apparent examples come from the intertidal, where the lower depth distributions of many species are set by predation (e.g. Luckens 1975). On land, a vivid evidence of the impact of consumption on vertical distribution is seen by the browsing of giraffes on trees (Woolnough & Du Toit 2001). However, although the probability of DSL observation at shallower depths is low in RSPD1, 3 and 5 (Fig. 4), they have been observed on occasion (< 10% probability), and we have sampled from an incomplete dataset both temporally (e.g. missing winter period in the Southern Ocean) and spatially (e.g. missing large sections of the Atlantic and eastern boundary upwelling systems).

The energy consumption by mesopelagic organisms that actively migrate can be divided into four different energy-consuming activities: i) foraging at the surface during the night (e.g. Dypvik & Kaartvedt 2013); ii) buoyancy control, via a gas bladder, lipid investment or by swimming (Proud et al. 2018); iii) predator evasion (Hays 2003), and iv) actively swimming during vertical migration (Brierley 2014). Variability in DSL depth directly impacts activities ii-iv to different degrees. For example, a gas-bladdered fish that re-inflates its gas bladder at depth to maintain neutral buoyancy, moving from a daytime position of 500 m down to 600 m (e.g. from RSPD1 to RSPD2), needs to produce more gas (due to higher pressure) to remain neutrally buoyant. The fish may also experience reduced predation from above by becoming inaccessible to some predators (e.g. King penguins), and more energy is required to vertically migrate. Foraging will also be impacted indirectly, as the energy remaining after other activities (ii-iv) may limit energy availability for foraging.

To investigate further, fine-scale predator-prey studies between access-restricted diving predators and DSLs should be conducted.

Low deep scattering layer vertical stability in Polar Regions

We have revealed two different DSL depth structures, Single-Shallow DSL (SS-DSL) and Double-Deep DSL (DD-DSL). The remaining cluster, RSPD6, found mainly in polar regions (Fig. 3), consisted of SPDs with low DSL vertical stability (Fig. 2) and relatively low intensity scattering layers (Fig. 4). Polar regions are cold, metabolic rates are reduced and life cycle stages are longer, reducing survival probability of larvae and hence lowering trophic efficiency (Rogers et al. 2011). There are relatively few mesopelagic fish species in the polar regions (3 spp. of *Myctophidae* in the Arctic and 19 in the Antarctic compared with > 100 spp. in the Indian Ocean, www.fishbase.org), which may lead to reduced productivity and ecosystem stability (Johnson et al. 1996). As the climate warms, fish diversity in polar regions may increase (e.g. Kaartvedt & Titelman 2018) and, with it, ecosystem stability and biomass may increase. In the Southern Ocean, a proportion of the fish population is believed to be migratory, spending their early life-cycle stages equatorward of the polar front (Saunders et al. 2017) and progressing towards the Antarctic shelf as adults, following Bergmann's Rule (Saunders & Tarling 2017). Since fish are relatively strong scatterers compared with zooplankton (Lavery et al. 2007), high spatial and temporal variability in community composition (proportion of zooplankton to fish) and biomass, along with patchy immigrations, could lead to the observed low vertical stability in DSL depth (see Table 1 and Fig. 2) and high variability in MVBS (Fig. 4, RSPD6).

437 *Partitioning the ocean*

438 The spatial coherence of the clusters (see Fig. 3) provides evidence that pelagic communities
439 as described using SSL characteristics (z, MVBS etc.) are distinct at the regional-scale. This is
440 particularly apparent in the south Indian Ocean region, where even though the underlying
441 data had the most extensive seasonal coverage (Table 1, RSPD4, SCI = 3.1), spatially
442 coherent regions formed. The spatial extent of the RSPDs varied geographically. Across the
443 North Atlantic, for example, the SSL structure varied substantially, shifting between 4
444 different RSPDs over a relatively small distance (Fig. 3). Anderson et al. (2005) reported
445 similar findings, observing high spatial and seasonal variability in DSL depth and echo
446 intensity, inferring that changes in oceanographic regimes were responsible. Conversely, in
447 the North Pacific, the SSL structure was more spatially stable, formed in the majority of a
448 single RSPD (Fig. 3).

449 Flynn and Marshall (2013) describe four zoogeographic regions off eastern Australia based
450 on lanternfish species occurrence data and related environmental variables (nitrate,
451 phosphate, oxygen, salinity and temperature). The four regions, Coral Sea, Subtropical
452 Lower water, Subantarctic, and Subtropical Convergence zone (South Tasman region)
453 correspond spatially to our RSPD5, 3, 6 and 1 respectively (Fig. 3 here and Flynn & Marshall's
454 (2013) Fig. 7). There is a stark difference between the Subantarctic region (RSPD6), also
455 defined by Longhurst (2007) as the Subantarctic water ring (SANT, Fig. 3), and the other
456 three RSPDs/zoogeographic regions, which all fall into the SS-DSL depth structure type and
457 are not as well-defined (Flynn & Marshall 2013, Fig. 7). In Flynn and Marshall's
458 bioregionalization model (2013), latitude is a significant covariate and they suggest that this
459 is a proxy for some unknown parameter, speculating that it could be related to food source

460 distribution, breeding, competitive exclusion or a consequence of larval transport barriers or
461 aggregating eddies. Here, the RSPDs are distinguished by their DSL echo intensity, which
462 increases from RSPD1 to RSPD6 (Table 1). This increase could be related to an increase in
463 biomass (Irigoien et al. 2014), and therefore related to food source distribution, or may just
464 be a consequence of differences in fish population scattering properties (Davison et al.
465 2015).

466 Recently, Proud et al. (2017), described a mesopelagic biogeography based on the daytime
467 depth of the principal DSL and 38 kHz backscattering intensity of observed daytime DSLs.
468 They predicted global mesopelagic backscatter using a simple linear model in which the
469 product of PP and temperature at the depth of the principle DSL was used as a predictor
470 variable. In this study, we have defined RSPDs based on the full water-column SSL structure
471 (not just the depth of the principle DSL), and quantified vertical stability of these structures.
472 By including consideration of the full water-column structure, ecological partitions could be
473 constructed that are more suitable for studies where fine-scale distribution of DSLs is
474 required e.g. foraging behaviour of deep-diving predators such as Elephant Seals and King
475 penguins in the Southern Ocean (Boersch-Supan et al. 2012).

476

477 *Mesopelagic components in Ecosystem models*

478 Recognition of the importance of the role of diel vertical migration in the carbon cycle has
479 increased over the last decade (Van De Waal et al. 2010, Doney et al. 2012, Passow &
480 Carlson 2012, Giering et al. 2014, Mitra et al. 2014), but modelling of these processes at
481 fine-scales has not developed as quickly. Traditional ecological models such as Ecopath
482 (Christensen & Walters 2004) do not explicitly define depth structure. Newer, more complex

models such as Atlantis (Fulton et al. 2011) have both diel variability and integrated depth levels. Modelers are now beginning to adapt their models. For example, SEAPOYDM (Lehodey et al. 2008) has recently been updated to included DVM behaviour and consideration of DSL depth structure related to euphotic depth (Lehodey et al. 2014). Accurate representation of the BCP in these models is important because output from these models feed into climate/Earth-system models.

Conclusions

Regional-scale, spatially and vertically coherent, water-column community depth structures can be derived from echosounder observations. In total, we describe six regional-scale sound scattering layer probability distributions from a near-global acoustic dataset. Other characteristic SSL depth structures may exist in regions for which we had no observations e.g. in the central and South Atlantic and the eastern boundary upwelling systems. Variability in deep scattering layer (DSL) number, depth, mean volume backscattering strength and vertical stability drive the characteristic forms of these day-night depth structures (Single-Shallow DSL and Double-Deep DSL) and these forms will likely impact the efficiency of the biological carbon pump and predator-prey interactions. The results presented here highlight the variability in fine-scale depth structure and vertical stability of the mesopelagic community throughout the global ocean. Both of these should be considered when partitioning the ocean's water-column into bioregions, and in the future development of ecological models.

Acknowledgements

We thank the British Oceanographic Data Centre, the Australian Integrated Marine Observing System, the British Antarctic Survey, and Dr. Phil Hosegood for providing echosounder data. This study has received support from the European H2020 International Cooperation project MESOPP (Mesopelagic Southern Ocean Prey and Predators, http://www.mesopp.eu/).

References

Aksnes DL, Røstad A, Kaartvedt S, Martinez U, Duarte CM, Irigoien X (2017) Light penetration structures the deep acoustic scattering layers in the global ocean. Sci Adv 3:1–6

Alvarino A (1965) Chaetognaths. Oceanogr Mar Biol An Annu Rev 3:115–194

Anderson CIH, Brierley AS, Armstrong F (2005) Spatio-temporal variability in the distribution of epi- and meso-pelagic acoustic backscatter in the Irminger Sea, North Atlantic, with implications for predation on Calanus finmarchicus. Mar Biol 146:1177–1188

Anderson TR, Martin AP, Lampitt RS, Trueman CN, Henson SA, Mayor DJ (2018) OUP accepted manuscript. ICES J Mar Sci

Andreeva IB, Galybin NN, Tarasov LL (2000) Vertical structure of the acoustic characteristics of deep scattering layers in the ocean. Acoust Phys 46:505–510

BAS (2015) Raw acoustic data collected by ship-borne EK60 echo sounder in the Scotia Sea (Oct - Dec 2006; Feb - Apr 2008; Mar - Apr 2009). Polar Data Centre; British Antarctic

526 Survey, Natural Environment Research Council; Cambridge, CB3 0ET, UK

527 Bestley S, Patterson TA, Hindell MA, Gunn JS (2008) Feeding ecology of wild migratory tunas
528 revealed by archival tag records of visceral warming. J Anim Ecol 77:1223–1233

529 Bianchi D, Galbraith ED, Carozza DA, Mislan KAS, Stock CA (2013) Intensification of open-
530 ocean oxygen depletion by vertically migrating animals. Nat Geosci 6:545–548

531 Bianchi D, Mislan KAS (2016) Global patterns of diel vertical migration times and velocities
532 from acoustic data. Limnol Oceanogr 61:353–364

533 Boersch-Supan PH, Boehme L, Read JF, Rogers AD, Brierley AS (2012) Elephant seal foraging
534 dives track prey distribution, not temperature: Comment on McIntyre et al. (2011).
535 Mar Ecol Prog Ser 461:293–298

536 Boyce DG, Lewis MR, Worm B (2010) Global phytoplankton decline over the past century.
537 Nature 466:591–596

538 Boyce DG, Lewis MR, Worm B (2012) Integrating global chlorophyll data from 1890 to 2010.
539 Limnol Oceanogr Methods 10:840–852

540 Brierley AS (2014) Diel vertical migration. Curr Biol 24:R1074–R1076

541 Briggs J (1974) Marine Zoogeograpghy. McGraw-Hill, New York

542 Brinton E (1962) The distribution of Pacific euphausiids. Berkeley Plan J 8:21–270

543 Brown RGB (1980) Seabirds as marine animals. In: Burger J, Olla BL, Winn HE (eds) Behavior
544 of Marine Animals. Plenum Press, New York, p 1–39

545 Charrassin JB, Bost CA (2001) Utilisation of the oceanic habitat by king penguins over the
546 annual cycle. Mar Ecol Prog Ser 221:285–297

547 Charrassin JB, Maho Y Le, Bost CA (2002) Seasonal changes in the diving parameters of king
548 penguins (Aptenodytes patagonicus). Mar Biol 141:581–589

549 Christensen V, Walters CJ (2004) Ecopath with Ecosim: Methods, capabilities and limitations.
550 Ecol Modell 172:109–139

551 Davison PC, Koslow JA, Kloser RJ (2015) Acoustic biomass estimation of mesopelagic fish:
552 backscattering from individuals, populations, and communities. ICES J Mar Sci 72:1413–
553 1424

554 Doney SC, Ruckelshaus M, Emmett Duffy J, Barry JP, Chan F, English CA, Galindo HM,
555 Grebmeier JM, Hollowed AB, Knowlton N, Polovina J, Rabalais NN, Sydeman WJ, Talley
556 LD (2012) Climate Change Impacts on Marine Ecosystems. Ann Rev Mar Sci 4:11–37

557 Dupont N, Klevjer TA, Kaartvedt S, Aksnes DL (2009) Diel vertical migration of the deep-
558 water jellyfish Periphylla periphylla simulated as individual responses to absolute light
559 intensity. Limnol Oceanogr 54:1765–1775

560 Dypvik E, Kaartvedt S (2013) Vertical migration and diel feeding periodicity of the
561 skinnycheek lanternfish (Benthosema pterotum) in the Red Sea. Deep Res Part I
562 Oceanogr Res Pap 72:9–16

563 Fennell S, Rose G (2015) Oceanographic influences on Deep Scattering Layers across the
564 North Atlantic. Deep Res Part I Oceanogr Res Pap 105:132–141

565 Flynn AJ, Kloser RJ (2012) Cross-basin heterogeneity in lanternfish (family Myctophidae)
566 assemblages and isotopic niches (δ 13C and δ 15N) in the southern Tasman Sea abyssal
567 basin. Deep Res Part I Oceanogr Res Pap 69:113–127

568 Flynn AJ, Marshall NJ (2013) Lanternfish (Myctophidae) Zoogeography off Eastern Australia:

569 A Comparison with Physicochemical Biogeography (V Laudet, Ed.). PLoS One 8:e80950

570 Fulton EA, Link JS, Kaplan IC, Savina-Rolland M, Johnson P, Ainsworth C, Horne P, Gorton R,
571 Gamble RJ, Smith ADM, Smith DC (2011) Lessons in modelling and management of
572 marine ecosystems: The Atlantis experience. Fish Fish 12:171–188

573 Giering SLC, Sanders R, Lampitt RS, Anderson TR, Tamburini C, Boutrif M, Zubkov M V.,
574 Marsay CM, Henson SA, Saw K, Cook K, Mayor DJ (2014) Reconciliation of the carbon
575 budget in the ocean's twilight zone. Nature 507:480–483

576 Godø OR, Samuelsen A, Macaulay GJ, Patel R, Hjøllo SS, Horne J, Kaartvedt S, Johannessen
577 JA (2012) Mesoscale eddies are oases for higher trophic marine life. PLoS One 7:e30161

578 Hartigan JA, Wong MA (1979) A K-Means Clustering Algorithm. Appl Stat 28:100–108

579 Hays GC (2003) A review of the adaptive significance and ecosystem consequences of
580 zooplankton diel vertical migrations. Hydrobiologia 503:163–170

581 Hazen EL, Johnston DW (2010) Meridional patterns in the deep scattering layers and top
582 predator distribution in the central equatorial Pacific. Fish Oceanogr 19:427–433

583 Hout MC, Papesh MH, Goldinger SD (2013) Multidimensional scaling. Wiley Interdiscip Rev
584 Cogn Sci 4:93–103

585 IMOS (2013) IMOS BASOOP sub facility, imos.org.au [accessed 1st June 2013]

586 Irigoien X, Klevjer TA, Røstad A, Martinez U, Boyra G, Acuña JL, Bode A, Echevarria F,
587 Gonzalez-Gordillo JI, Hernandez-Leon S, Agusti S, Aksnes DL, Duarte CM, Kaartvedt S
588 (2014) Large mesopelagic fishes biomass and trophic efficiency in the open ocean. Nat
589 Commun 5:3271

590 Johnson KH, Vogt KA, Clark HJ, Schmitz OJ, Vogt DJ (1996) Biodiversity and the productivity
591 and stability of ecosystems. Trends Ecol Evol 11:372–377

592 Jónasdóttir SH, Visser AW, Richardson K, Heath MR (2015) Seasonal copepod lipid pump
593 promotes carbon sequestration in the deep North Atlantic. Proc Natl Acad Sci
594 112:12122–12126

595 Kaartvedt S, Titelman J (2018) Planktivorous fish in a future Arctic Ocean of changing ice and
596 unchanged photoperiod. ICES J Mar Sci

597 Klevjer TA, Irigoien X, Røstad A, Fraile-Nuez E, Benítez-Barrios VM, Kaartvedt. S (2016) Large
598 scale patterns in vertical distribution and behaviour of mesopelagic scattering layers.
599 Sci Rep 6:19873

600 Klevjer TA, Torres DJ, Kaartvedt S (2012) Distribution and diel vertical movements of
601 mesopelagic scattering layers in the Red Sea. Mar Biol 159:1833–1841

602 Kloser RJ, Ryan TE, Young JW, Lewis ME (2009) Acoustic observations of micronekton fish on
603 the scale of an ocean basin: potential and challenges. ICES J Mar Sci 66:998–1006

604 Knutsen T, Wiebe PH, Gjøsæter H, Ingvaldsen RB, Lien G (2017) High Latitude Epipelagic and
605 Mesopelagic Scattering Layers—A Reference for Future Arctic Ecosystem Change. Front
606 Mar Sci 4:1–21

607 Koslow JA, Kloser RJ, Williams A (1997) Pelagic biomass and community structure over the
608 mid-continental slope off southeastern Australia based upon acoustic and midwater
609 trawl sampling. Mar Ecol Prog Ser 146:21–35

610 Kruskal JB (1964) Multidimensional scaling by optimizing goodness of fit to a nonmetric
611 hypothesis. Psychometrika 29:1–27

612 Lavery AC, Wiebe PH, Stanton TK, Lawson GL, Benfield MC, Copley N (2007) Determining
613 dominant scatterers of sound in mixed zooplankton populations. J Acoust Soc Am
614 122:3304–3326

615 Lehodey P, Conchon A, Senina I, Domokos R, Calmettes B, Jouanno J, Hernandez O, Kloser R
616 (2014) Optimization of a micronekton model with acoustic data. ICES J Mar Sci
617 72:1399–1412

618 Lehodey P, Senina I, Murtugudde R (2008) A spatial ecosystem and populations dynamics
619 model (SEAPODYM) – Modeling of tuna and tuna-like populations. Prog Oceanogr
620 78:304–318

621 Longhurst AR (2007) Ecological Geography of the Sea, Second Edi. Academic Press, San
622 Diego

623 Luckens PA (1975) Predation and intertidal zonation of barnacles at leigh, New Zealand.
624 New Zeal J Mar Freshw Res 9:355–378

625 Maclennan DN, Fernandes PG, Dalen J (2002) A consistent approach to definitions and
626 symbols in fisheries acoustics. ICES J Mar Sci 59:365–369

627 McIntyre T, Bruyn PJN de, Ansorge IJ, Bester MN, Bornemann H, Plötz J, Tosh CA (2010) A
628 lifetime at depth: Vertical distribution of southern elephant seals in the water column.
629 Polar Biol 33:1037–1048

630 Mitra A, Flynn KJ, Burkholder JM, Berge T, Calbet A, Raven JA, Granéli E, Glibert PM, Hansen
631 PJ, Stoecker DK, Thingstad F, Tillmann U, Våge S, Wilken S, Zubkov M V. (2014) The role
632 of mixotrophic protists in the biological carbon pump. Biogeosciences 11:995–1005

633 Mori Y, Boyd IL (2004) The behavioral basis for nonlinear functional responses and optimal

foraging in antarctic fur seals. Ecology 85:398–410

New LF, Clark JS, Costa DP, Fleishman E, Hindell MA, Klanjšček T, Lusseau D, Kraus S, McMahon CR, Robinson PW, Schick RS, Schwarz LK, Simmons SE, Thomas L, Tyack P, Harwood J (2014) Using short-term measures of behaviour to estimate long-term fitness of southern elephant seals. Mar Ecol Prog Ser 496:99–108

Oliver MJ, Irwin AJ (2008) Objective global ocean biogeographic provinces. Geophys Res Lett 35:L15601

Olsson O, North AW (1997) Diet of the King Penguin Aptenodytes patagonicus during three summers at South Georgia. Ibis (Lond 1859) 139:504–512

Parekh P, Dutkiewicz S, Follows MJ, Ito T (2006) Atmospheric carbon dioxide in a less dusty world. Geophys Res Lett 33:L03610

Passow U, Carlson CA (2012) The biological pump in a high CO2 world. Mar Ecol Prog Ser 470:249–271

Proud R, Cox MJ, Brierley AS (2017) Biogeography of the Global Ocean's Mesopelagic Zone. Curr Biol 27:113–119

Proud R, Cox MJ, Wotherspoon S, Brierley AS (2015) A method for identifying Sound Scattering Layers and extracting key characteristics (A Tatem, Ed.). Methods Ecol Evol 6:1190–1198

Proud R, Handegard NO, Kloser RJ, Cox MJ, Brierley AS (2018) From siphonophores to deep scattering layers: uncertainty ranges for the estimation of global mesopelagic fish biomass. ICES J Mar Sci

655 Rogers AD, Johnston NM, Murphy EJ, Clarke A (2012) Antarctic Ecosystems (AD Rogers, NM
656 Johnston, EJ Murphy, and A Clarke, Eds.). John Wiley & Sons, Ltd, Chichester, UK

657 Saunders RA, Collins MA, Stowasser G, Tarling GA (2017) Southern Ocean mesopelagic fish
658 communities in the Scotia Sea are sustained by mass immigration. Mar Ecol Prog Ser
659 569:173–185

660 Saunders RA, Tarling GA (2018) Southern Ocean Mesopelagic Fish Comply with Bergmann's
661 Rule. Am Nat 191:343–351

662 Sayre RG, Wright DJ, Breyer SP, Butler KA, Graafeiland K Van, Costello MJ, Harris PT, Goodin
663 KL, Guinotte JM, Basher Z, Kavanaugh MT, Halpin PN, Cressie N, Aniello P, Frye CE,
664 Society TO (2017) A Three-Dimensional Mapping of the Ocean Based on Environmental
665 Data. Oceanography 30:90–103

666 Scheffer A, Trathan PN, Collins M (2010) Foraging behaviour of King Penguins (Aptenodytes
667 patagonicus) in relation to predictable mesoscale oceanographic features in the Polar
668 Front Zone to the north of South Georgia. Prog Oceanogr 86:232–245

669 Schnetzer A, Steinberg DK (2002) Active transport of particulate organic carbon and nitrogen
670 by vertically migrating zooplankton in the Sargasso Sea. Mar Ecol Prog Ser 234:71–84

671 Schoener TW (1979) Generality of the Size-Distance Relation in Models of Optimal Feeding.
672 Am Nat 114:902–914

673 Scott F, Blanchard JL, Andersen KH (2014) mizer: An R package for multispecies, trait-based
674 and community size spectrum ecological modelling. Methods Ecol Evol 5:1121–1125

675 Semina HJ (1997) An outline of the geographical distribution of oceanic phytoplankton. In:
676 Advances in Marine Biology.p 527–563

677 Spalding MD, Agostini VN, Rice J, Grant SM (2012) Pelagic provinces of the world: A
678 biogeographic classification of the world's surface pelagic waters. Ocean Coast Manag
679 60:19–30

680 Sugar C (1998) Techniques for clustering and classification with applications to medical
681 problems. Stanford University, Stanford

682 Sutton TT, Clark MR, Dunn DC, Halpin PN, Rogers AD, Guinotte J, Bograd SJ, Angel M V.,
683 Perez JAA, Wishner K, Haedrich RL, Lindsay DJ, Drazen JC, Vereshchaka A, Piatkowski U,
684 Morato T, Błachowiak-Samołyk K, Robison BH, Gjerde KM, Pierrot-Bults A, Bernal P,
685 Reygondeau G, Heino M (2017) A global biogeographic classification of the mesopelagic
686 zone. Deep Res Part I Oceanogr Res Pap 126:85–102

687 Trebilco R, Baum JK, Salomon AK, Dulvy NK (2013) Ecosystem ecology: Size-based
688 constraints on the pyramids of life. Trends Ecol Evol 28:423–431

689 UNESCO (2009) Global Open Oceans and Deep Seabed (GOODS) - biogeographic
690 classification.

691 Vacquié-Garcia J, Guinet C, Laurent C, Bailleul F (2015) Delineation of the southern elephant
692 seal's main foraging environments defined by temperature and light conditions. Deep
693 Res Part II Top Stud Oceanogr 113:145–153

694 Vinogradov M. (1968) Vertical distribution of oceanic zooplankton. Isr Progr Sci Transl 1970
695 (Original Acad Nauk SSSR, Inst Okeanol)

696 Waal DB Van De, Verschoor AM, Verspagen JMH, Donk E Van, Huisman J (2010) Climate-
697 driven changes in the ecological stoichiometry of aquatic ecosystems. Front Ecol
698 Environ 8:145–152

699 Watling L, Guinotte J, Clark MR, Smith CR (2013) A proposed biogeography of the deep
700 ocean floor. Prog Oceanogr 111:91–112

701 Woolnough A, Toit J Du (2001) Vertical zonation of browse quality in tree canopies exposed
702 to a size-structured guild of African browsing ungulates. Oecologia 129:585–590

703

704

705

706

707

708

709

710

711

712

713

714

715

716

717

Figures

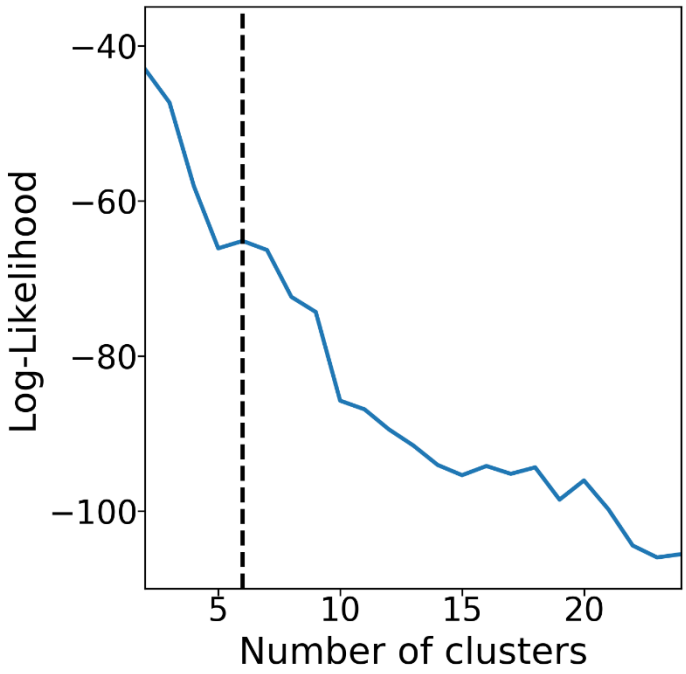

Fig. 1. Change in Log-Likelihoods by number of k-means clusters. Six clusters were selected (indicated by a black dashed line) on the basis that an elbow-like feature with an increasing Log-Likelihood at that scale diverged from the otherwise decreasing linear trend.

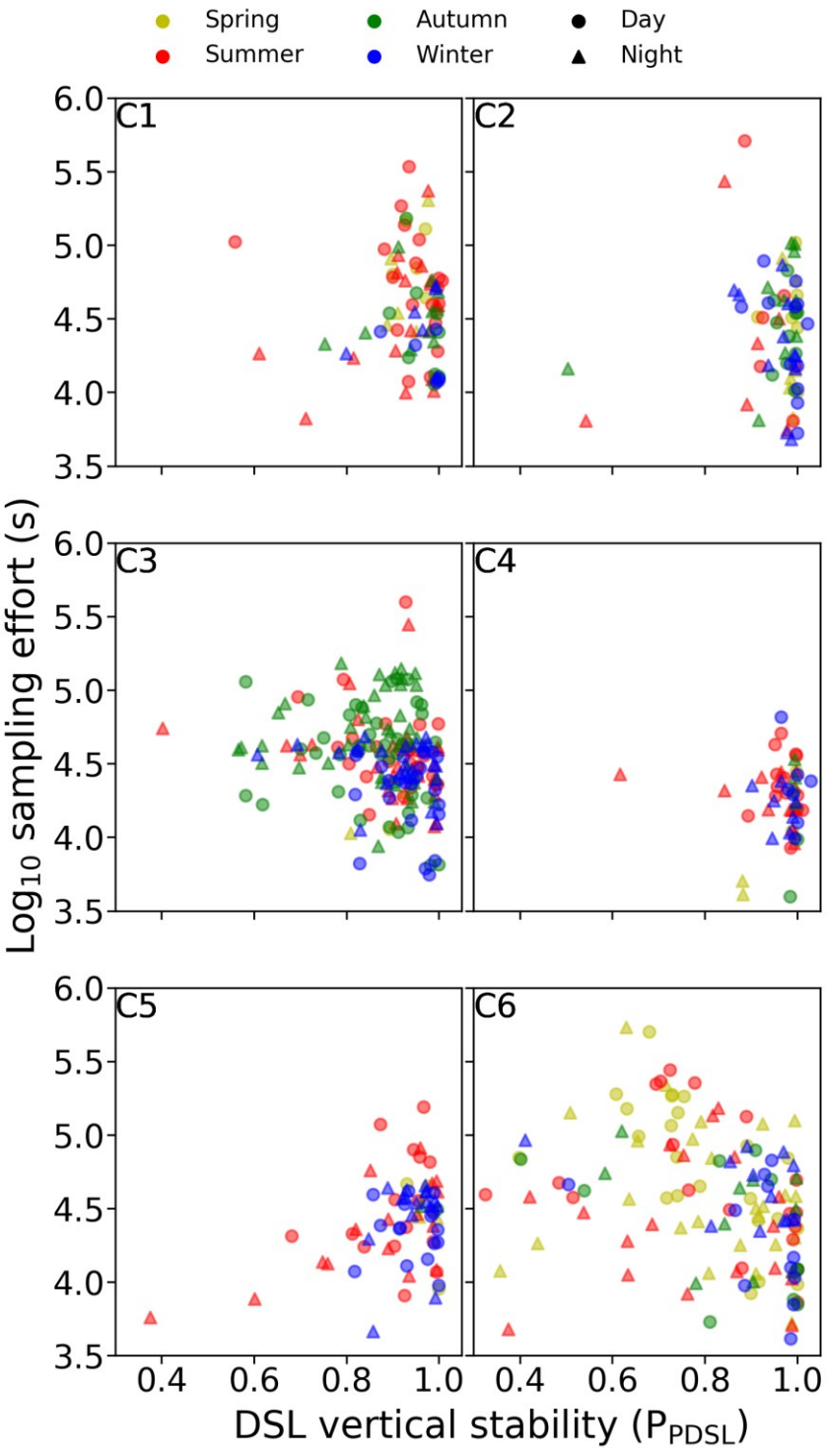

723

724 Fig. 2. Deep scattering layer (DSL) vertical stability, defined as the maximum probability of

725 DSL observation (P_{PDSL}) and sampling effort (echosounder observations) by season, diel state

726 and cluster for each local-scale (300 by 300 km cell) sound scattering layer probability

727 distribution.

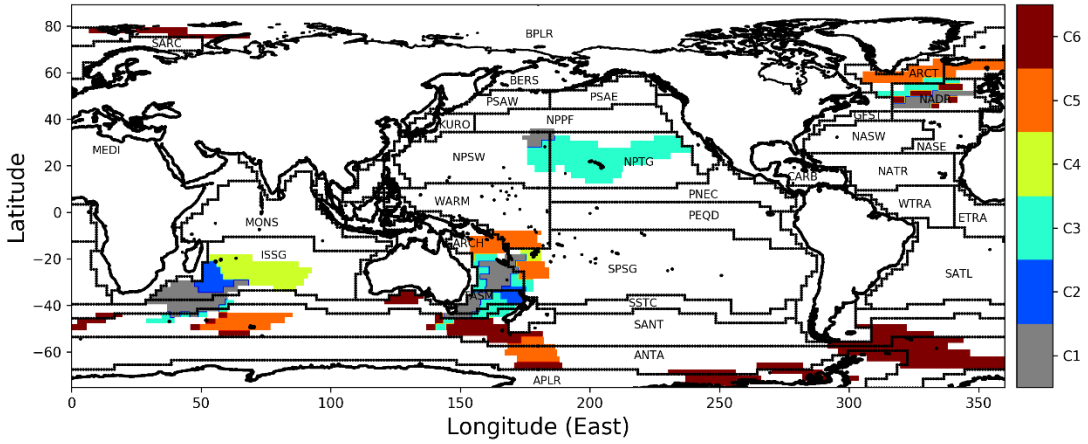

728

729 Fig. 3. Geographical distribution of echosounder data (coloured cells) and sound scattering

730 layer probability distribution cluster membership (C1 to C6). Longhurst's (2007) pelagic

731 ocean provinces are shown for reference, labelled by their short-name.

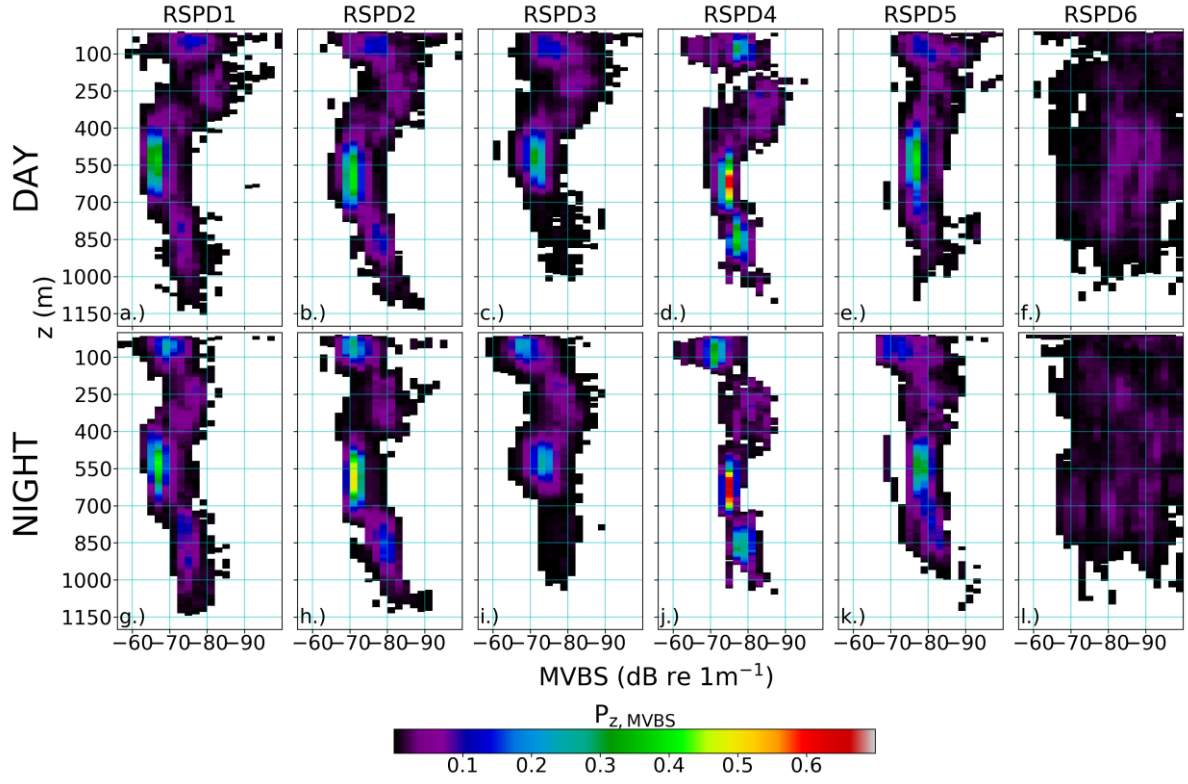

732

733 Fig. 4. Regional-scale sound scattering layer probability distributions (RSPDs) plotted in

734 depth-MVBS space. Each RSPD has a day and night component. $P_{z,MVBS}$ is the probability of

735 observing a sound scattering layer of a given depth (z) and MVBS value. White regions

indicate a probability of 0 i.e. no sound scattering layers were observed in the region represented by the RSPD for those specific depth-MVBS combinations.

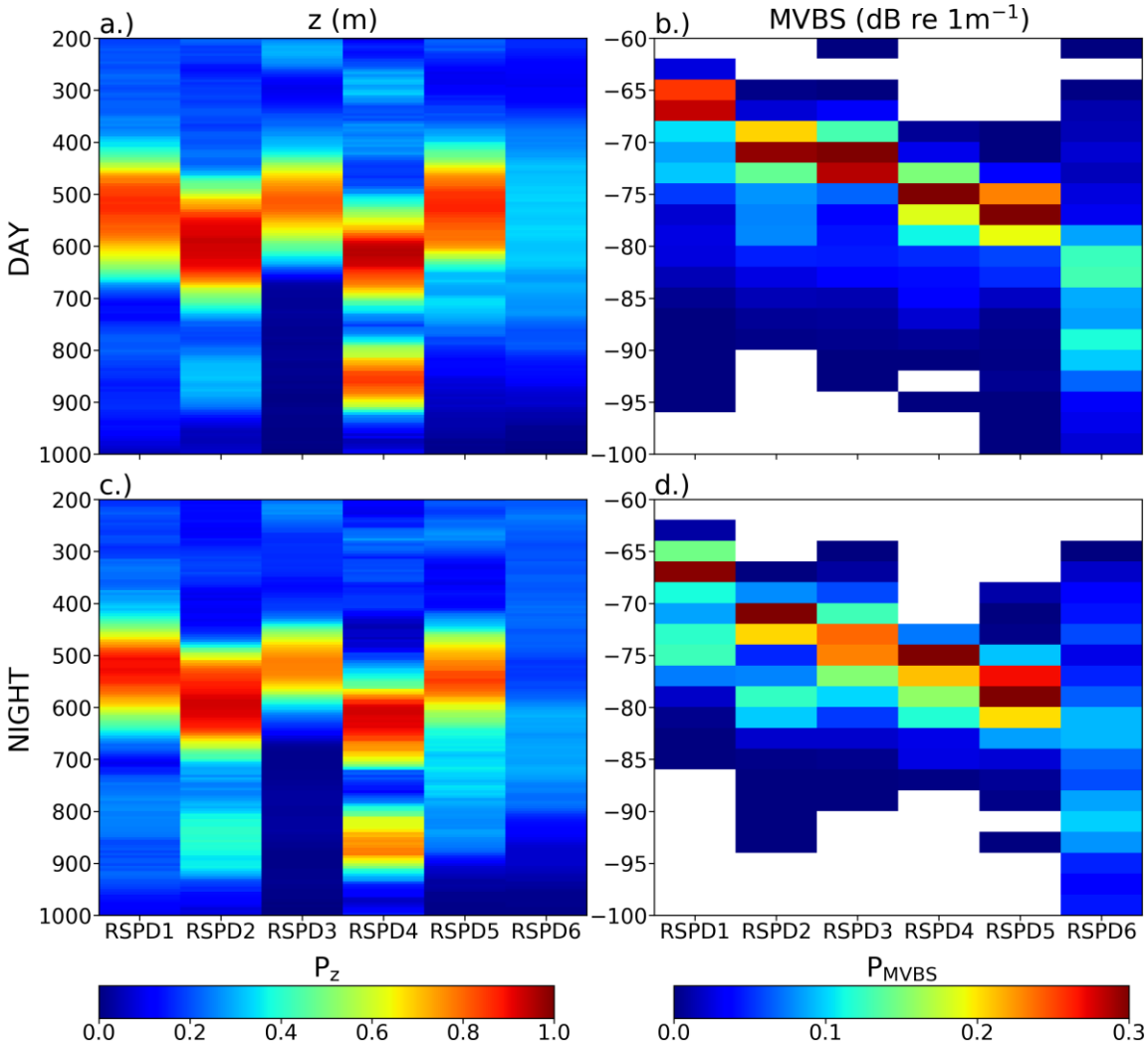

Fig. 5. Stability of deep scattering layer (DSL; sound scattering layer > 200 m) depth and mean volume backscattering strength (MVBS) for each regional-scale sound scattering layer probability distribution (RSPD). P_z (panels a and c), is the probability of DSL observation by depth and, P_{MVBS} (panels b and d), is the probability of an observed DSL having a specific MVBS value.

746 **Tables**

		Day				Night			
RSPD	SCI (1-4)	Z_{PDSL} (m)	$MVBS_{PDSL}$ (dB re $1m^{-1}$)	s_{meso} (m^2 nmi^{-2})	s_{epi} (m^2 nmi^{-2})	Z_{PDSL} (m)	$MVBS_{PDSL}$ (dB re $1m^{-1}$)	s_{meso} (m^2 nmi^{-2})	s_{epi} (m^2 nmi^{-2})
1	2.1	510 (0.87)	-67 (0.23)	2692	139	525 (0.91)	-67 (0.27)	2173	479
2	2.9	590 (0.94)	-71 (0.25)	1103	143	585 (0.93)	-71 (0.33)	848	368
3	1.7	510 (0.82)	-73 (0.25)	679	121	510 (0.77)	-73 (0.2)	390	650
4	3.1	615 (0.95)	-75 (0.31)	517	232	605 (0.97)	-75 (0.31)	370	511
5	1.8	530 (0.87)	-77 (0.35)	287	44	545 (0.85)	-79 (0.26)	215	280
6	1.8	625 (0.44)	-83 (0.12)	95	19	615 (0.46)	-91 (0.09)	152	35

747

748 Table 1. Regional-scale sound scattering layer (SSL) probability distribution (RSPD)
749 characteristics ranked in accordance to their daytime s_{meso} values. SCI is the seasonal
750 coverage index, which ranges between 1 (single season) and 4 (all seasons uniformly
751 represented). Z_{PDSL}, is the principal (most common) deep scattering layer (DSL; SSL deeper
752 than 200 m) depth, $MVBS_{PDSL}$, is the most likely MVBS value for the principal DSL, given that
753 a DSL is observed, and s_{meso} and s_{epi}, are the nautical area scattering coefficient (NASC)
754 values for SSLs found within the mesopelagic (200 – 1000 m) and epipelagic (0 – 200 m)
755 zones respectively. Bracketed values are stability of principal DSL depth (P_{PDSL}) and principal
756 DSL MVBS value (P_{PMVBS}). Day-to-night increase in NASC in the epipelagic and decrease in the
757 mesopelagic implies DVM (shaded cells).

758